ARTICLE

The effect of spin polarization on the electron transport of molecular wires with diradical character

Accepted 08th Feb 2021

DOI: 10.1039/D0CP06321E

Nicolás Ramos-Berdullas,[a] Sara Gil-Guerrero,[a] Ángeles Peña-Gallego[a] and Marcos Mandado*[a]

Some of the most promising materials for application in molecular electronics and spintronics are based on diradical chains. Herein, the proposed relation between increasing conductance with length and diradical character is revisited using ab initio methods that account for the static electron correlation effects. Electron transmission was previously obtained from restricted single determinant wavefuntions or tight-binding approximations, which are unable to account for static correlation. Broken Symmetry Unrestricted Kohn-Sham Density Functional Theory (BS-UKS-DFT) in combination with electron transport analysis based on electron deformation orbitals (EDOs) reflects an exponential decay of the electrical conductance with length. Also, other important effects such as quantum interference are correctly accounted for, leading to a decrease of the conductance as the diradical character increases. As a proof-of-concept, the electrical conductance obtained from BS-UKS-DFT and CASSCF(2,2) wavefunctions were compared in diradical graphene strips in the frame of the pseudo-π approach, obtaining very similar results.

1. Introduction

Quantum chemical simulations of electron and spin transport represent nowadays a key ingredient for the efficient design of molecular devices with different applications in Nanoelectronics and Spintronics fields.[1-14] Endorsed by recent experimental achievements, organic polymers,[15-25] cumulene chains,[26,27] graphene strips[28-33] and non-Kekulean polycyclic aromatic hydrocarbons[34-36] are molecular materials with an extraordinary potentiality. Most of them display polyradical character with a ground state of high multireference character even in chains of medium-length. Thus, they display strong static correlation, representing challenging systems from a computational point of view. Besides the complications inherent in determining the electronic structure of strongly correlated systems, an electron transport theory that properly handles multireference character has not been developed yet. Then, single reference quantum chemical methods, such as those based on Kohn-Sham Density Functional Theory (KS-DFT), or approximated tight-binding Hamiltonians have been employed to study the transport properties in molecular chains with diradical character.[37-48] Unfortunately, the behavior might radically change when the static correlation effects are accounted for, as shown by indirect measures of the electrical conductance, such as atom-atom localization tensors or delocalization indices.[49,50]

A very illustrative example of the problems inherent to single reference KS-DFT to study the electron transport in molecular chains with diradical character is the particular case of dimethylene polyphenylene, polypirrole, polyfuran and polythiophene polymers. Thus, KS-DFT outcomed an extraordinary behavior where the exponential decay of the electrical conductance with respect to the chain length is reversed.[39,40,42] Hückel (tight-binding) analysis, together with a valence bond model based on the counting of Kékule structures, related this behavior to the diradical character.[42] This tight-binding analysis also predicted the existence of an optimal conductance for a certain diradical character, after which the conductance will decrease as the diradical character increases. Further KS-DFT calculations in partially diradical chains supported the idea that increasing the diradical character through chemical control could increase the electrical conductance of a given molecular chain.[43-44] A subsequent work showed that this extraordinary behavior stems from a length-increasing superexchange transport mechanism associated with quasi-degenerated HOMO and LUMO states localized at both chain ends.[49] However, further multireference calculations yielded partially occupied states, each localized at one chain end, preventing the formation of the electron transport channels that give rise to the superexchange mechanism at KS-DFT level.[49,50] Since the calculation of the electrical conductance at multireference level was still not available, qualitative predictions were settled on the basis of electron localization/delocalization measures.[50] However, a more solid proof based on explicit calculations of the electrical conductance is needed in order to shed more light on the role played by the diradical character on the electron transport.

Fortunately, unrestricted KS-DFT (UKS-DFT) methods with spin and spatial symmetry breaking incorporate, quite reliably, static

[a] Department of Physical Chemistry, University of Vigo, Lagoas-Marcosende s/n, 36310, Vigo, Spain

Electronic Supplementary Information (ESI) available: [EDOs formulation in single and multideterminant wavefunctions; comparison of electrical conductance in OS, T and BS states; OS, T and BS energy differences; Nu values in graphene strips; electrical conductance in tetraphenyl cumulenes]. See DOI: 10.1039/x0xx00000x

and dynamic electron correlation effects in diradical systems with an open-shell singlet (OS) ground state.[51] This methodology is commonly known as Broken-Symmetry[52,53] Unrestricted KS-DFT (BS-UKS-DFT). Examples of the successful application of BS-UKS-DFT in diradical para-dimethylene polyphenylenes,[54] graphene strips[55] or non-Kekuléan PAHs can be found in the recent literature.[56,57] Since broken-symmetry (BS) solutions are not eigenstates of the $\mathbf{S}^2$ operator, BS-UKS-DFT often provides incorrect spin densities and is not suitable for the calculation of spin transport.[58] On the contrary, it is suitable for the study of the electron transport in OS states of perfect diradical chains (see the ESI). The method is further checked by comparing the results with those obtained from multireference wavefunctions, which are applied for the simulation of the electron transport in molecular junctions for the first time.

2. Methodology

In this work, the electrical conductance has been explicitly determined using the Landauer formalism[59] in the closed-shell (CS) and BS solutions of different polymeric chains and graphene strips. The electron transmission was calculated using electron transport channels built with electron deformation orbitals (EDOs).[60,61] Further details about the methodology employed to calculate the electrical conductance are given in the ESI.

Geometry optimizations and wave function calculations were carried out using the same computational levels employed in previous studies. Thus, the PBEPBE functional and the cc-pVDZ basis set was employed for cumulenes, but the B3LYP functional and the same basis set was employed for dimethylene polyphenylene, all-trans dimethylene polyfuran, all-trans dimethylene polythiophene and the graphene strips. The gold atoms were treated with the LANLD2Z combination of double zeta basis set + pseudo potential. These calculations were done with the Gaussian09 program,[62] whereas the electrical conductance was obtained with an own Fortran 90 implementation of the EDOs method. Visualization of the electron transport channels was done with the Gaussview interface program.[63] In order to verify the performance of BS-UKS-DFT against a more appropriate but largely more computationally demanding multireference scenario, we have compared the electrical conductance obtained from BS-UKS-DFT with that obtained from calculations using the Complete Active Space Self-Consistent Field (CASSCF) method in a series of graphene strips (those exhibiting a clear diradical character). Among the different criteria for measuring diradical character in the graphene strips, we have employed here the number of effectively unpaired electrons (*Nu*) proposed by Head-Gordon[64] within the MO/CASSCF scheme.

Additionally, electron transmission calculations were performed using Non-Equilibrium Green Functions (NEGF) in combination with RKS-DFT and BS-UKS-DFT for the smaller chains of each graphene strip. Using the electronic structure calculations performed with Gaussian09 as input, we have employed the Artaios code[65] for the transmission calculations.

3. Results and discussion

The first polymeric chain discussed in this work is the dimethylene polyphenylene. This is not a stable polymer but it is an ideal system to show the performance of BS-UKS-DFT. Its clear diradical character, even for the shortest chains, makes it the perfect model to illustrate the differences expected in general between the electron transport of CS and OS. Adiabatic energy differences between CS, BS and triplet (T) state are collected in Table S1 and indicate BS and T lays below the energy of CS for chains with n > 2. The electrical conductance is represented in Fig. 1 against the number of units for both states (for chains with $3 \leq n \leq 12$).

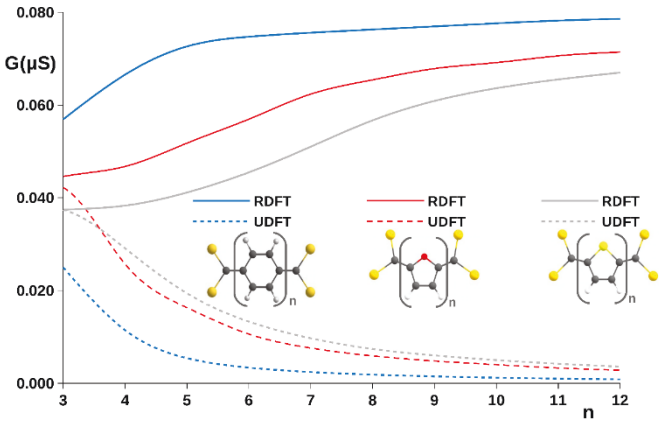

Fig. 1 Electrical conductance vs the number of aromatic units for BS (dashed lines) and CS (solid lines) of dimethylene polyphenylene (blue), dimethylene polyfurane (yellow) and dimethylene polythiophene (grey) chains.

Whereas for CS the representation shows a large and length increasing conductance, for the most stable BS, the conductance is drastically reduced and decreases with the chain length. The reason for such different behaviors is found on the characteristics of the electron transport channels in both cases. As shown and discussed in previous works,[39,49] in CS, the combination of the HOMO and LUMO MOs gives rise to a dominant channel, highly polarized at the molecule-metal contacts, whose weight and polarization increase with the chain length. On the contrary, in BS the formation of this channel is no longer possible due to the spatial symmetry breaking of the frontier molecular spin orbitals.

In Fig. 2, the main transmission channels and the MOs involved in their formation are shown for CS and BS of the chain with n = 6. As it can be seen, the localization of the HOMO and LUMO at the chain ends and their almost negligible energy gap in CS allows the formation of a highly conducting channel polarized at the molecule-metal contacts. As discussed in reference 49, the electron transport in this channel occurs via superexchange mechanism. However, in BS, the mixing of frontier orbitals produces pairs of alpha and beta occupied-unoccupied molecular spin orbitals polarized at opposite sides (see Fig. 2).

Thus, the alpha and beta transport channels that arise from the combination of these pairs will mostly cancel each other, giving rise to a global channel (the one with real physical sense) whose conductance is much lower than that of CS.

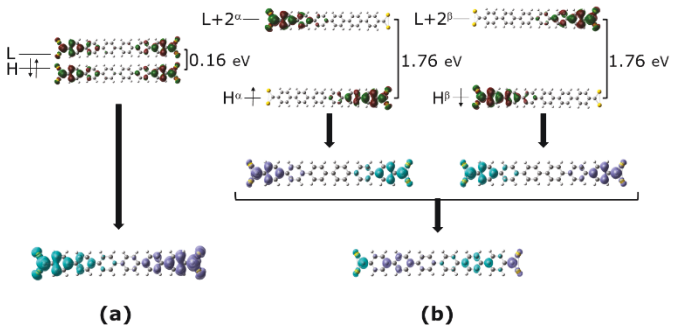

Fig. 2 Formation of electron transport channels in CS (a) and BS (b) of a dimethylene polyphenylene chain with n = 6. MOs involved in the respective channels, their energy gaps and the densities of the channels (blue negative, violet positive) are shown in the figure. Isosurface values for the representations are: 0.02 for the MO_S, $1{\cdot}10^{-3}$ for the spin channels and $1{\cdot}10^{-5}$ for the electron channels.

In Fig. 1, the representations of the conductance vs the number of units for dimethylene polyfurane and dimethylene polythiophene chains are also included. Exactly the same behavior found in polyphenylene chains is found for these two cases. Additionally, the comparison between the three polymeric chains sheds some light on the role played by aromaticity in the electron transport. Thus, using RKS-DFT in combination with EDOs, we can see that the larger the aromaticity of the monomers the larger the conductance, following the order, benzene > furan > thiophene, in agreement with previous calculations.[39] On the contrary, when the effect of the spin polarization is introduced in BS the opposite trend is found. This trend reversal is due again to the destruction of the channel responsible of the superexchange electron transport, which, in the wrong picture provided by RKS-DFT calculations, is favoured by the aromaticity of the monomer units.

The next class of polymeric chains studied are quinoid-cumulenes. In Fig. 3, the conductance is represented versus the number of C=C units for cumulene chains containing an aromatic group in the center, benzene or anthracene. These chains have a great potentiality for electronic applications due to their rigid structure and a smooth decay of the electrical conductance with the chain length predicted by RKS-DFT calculations.[38] Very recent experiments using Scanning Tunneling Microscopy (STM) even point to a small increase of the conductance in substituted cumulene chains.[26,27] This happens in tetraphenyl cumulenes attached to gold electrodes by methyl thiol linkers. In this work, the CS wave function for these tetraphenyl cumulenes has been found to be stable, so that no BS solution has been obtained. Therefore, they will not be discussed in the body of this letter but an analysis of the lower energy spin states and the conductance using EDOs have been included in the ESI. On the contrary, the two quinoid-cumulene chains included here display a non-negligible diradical character, which increases with the chain length (see ESI for details).

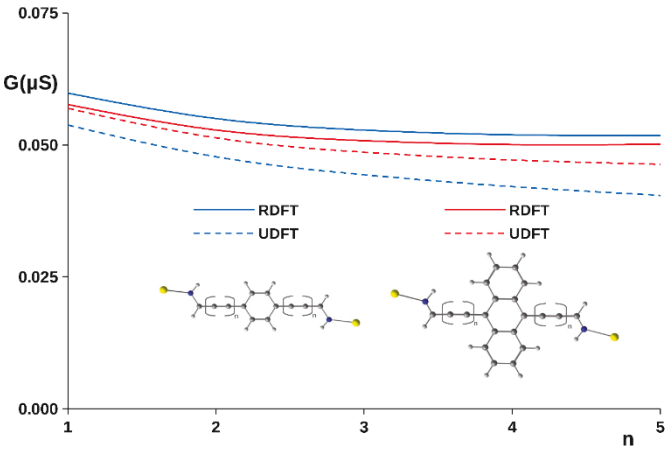

Fig. 3 Electrical conductance vs the number of C=C units (in each side) for BS (dashed lines) and CS (solid lines) of quinoid-cumulenes with phenyl (black) and anthracene (grey) as central aromatic units.

In Fig. 3, the electrical conductance vs the number of units for the series of cumulenes is depicted. At the RKS-DFT level, both chains display parallel behaviors with a subtle decrease in the conductance with the length in the short chains, asymptotically converging to a constant value for long chains. With respect to the central aromatic group, the conductance follows the order benzene > anthracene. Since the cyclic electron delocalization of the central ring decreases with the number of phenyl rings in the series of acenes, this conductance order is certainly an unexpected result. It points out to a constructive quantum interference effect exerted by the aromatic units. On the contrary, BS-UKS-DFT calculations reveal again this order is a simple artifact of the erroneous electronic structure provided by the single determinant closed-shell wavefunction. Thus, the conductance decreases following the order anthracene > benzene due to the destructive quantum interference effects exerted by the respective central aromatic groups. Moreover, the asymptotic behavior observed for the conductance vs the number of C=C units at RKS-DFT level is attenuated in BS-UKS-DFT, although the decrease in conductance is still quite slow, confirming the unusual and extraordinary conducting ability of cumulene chains.[38,26,27]

The last set of polyradicals studied are finite-size graphene strips. Here, we have chosen three armchair graphene strips with different width (N = 5,7,9), being N the number of carbon atoms along its width. This corresponds to strips with naphthalene, anthracene and tetracene as repeating units. The chain length is again represented by the number of these units, n (see Fig. 4), with $2 \le n \le 20$. No BS solution has been found for strips with N = 5, so that the ground state corresponds to CS in chains with $n \le 20$. Thus, the UKS-DFT and RKS-DFT calculations lead to the same representation of the conductance (Fig. 4). No reversed exponential decay of the electrical conductance with the chain length is observed here since the frontier MOs display a significant energy gap (the smallest one is 1.1 eV and

corresponds to n = 20) and are not strongly localized at the strip ends.[50]

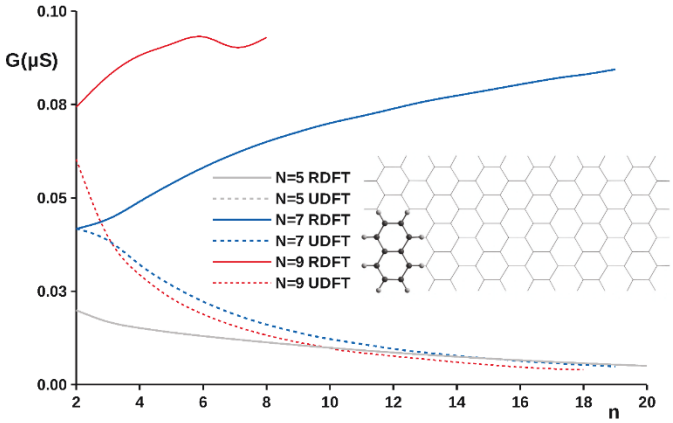

Fig. 4 Electrical conductance vs the number of polyacene units for BS (dashed lines) and CS (solid lines) of armchair graphene strips with N = 5 (grey), 7 (blue) and 9 (red).

For N = 7, CS is the ground state only when n = 2. As it can be seen in Table S3, BS energy lays below the CS when n ≥ 3. Thus, the ground state for these graphene strips is an OS, whose diradical character rapidly increases with the length. This leads to huge differences in the calculated electrical conductance as it can be observed in Fig. 4. An increase of the conductance with the strip length is predicted at the RKS-DFT level whereas the expected decay is recovered when the system is properly treated with BS-UKS-DFT.

For N = 9, a non-negligible diradical character is observed even in the smallest strip with n = 2 (see Table S4). The energy of BS lays below CS for all the strips (see Table S3). The representations of the electrical conductance against n are included in Fig. 4. As in the previous case, BS-UKS-DFT calculations show the expected exponential decay of the conductance whereas RKS-DFT wrongly predicts the reversed trend. The strong instabilities of the RKS-DFT wave functions for chains with n > 8 led to convergence problem in the calculations. This is the reason why the RDFT representation in Fig. 4 only contains values from n = 2 to n = 8.

Transmission calculations were also performed using NEGF in combination with RKS-DFT and BS-UKS-DFT (Fig. 5) for the smaller chains of the series N = 5, 7 and 9. The obtained results also reflect a change from reversal to normal decay of the electron transmission with the chain length for N = 7 and 9 when BS-KS-DFT is employed instead of RKS-DFT. Moreover, no changes are observed for N = 5 as the unrestricted calculations converge to the restricted solution. This is a proof that the conclusions of this work are independent of the method employed for the analysis of the electron transport.

At this point, we have shown that the extraordinary reversal of the conductance/length relation previously predicted for the organic chains studied here was the result of the erroneous description of the system provided by a single restricted KS determinant. Also, we have seen that spin symmetry breaking allows recovering the correct trend and probably a quantitative solution. The latter, however, requires further examination in order to affirm that BS-UKS-DFT is a cheap but reliable method for the study of the electron transport in diradical chains. A way to proof this is by comparison of the BS-UKS-DFT results with those obtained from a multireference wavefunction. Among the chains investigated in this work, the graphene strips with N = 9 discussed above are those with highest diradical character. CASSCF calculations using a minimal active space, which in this case involves only two electrons and two orbitals, reflect that all the strips have a number of effectively unpaired electrons (N_U) larger than 1.50 when n > 2, reaching a perfect diradical character (N_U = 2.00) for n ≥ 7 (see Table S4). Therefore, we have selected these chains to compare the electrical conductance obtained with BS-UKS-DFT and CASSCF. It is worth to notice here that larger active spaces were considered in reference 50, only for chains with 2 ≤ n ≤ 6 in this graphene strip. The results did not change significantly with respect to the minimal active space when n>3 since the MOs responsible of the multireference character are just the HOMO and LUMO.

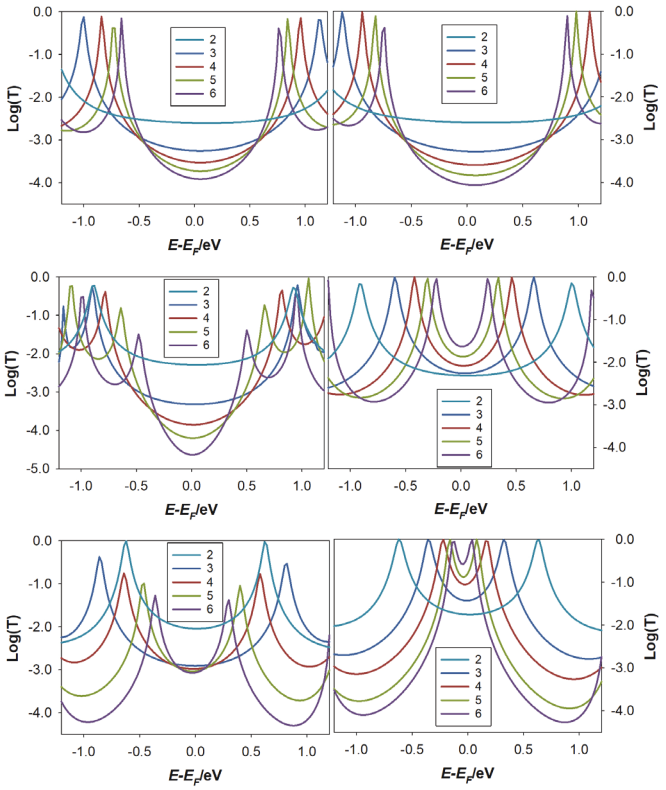

Fig. 5 Electron transmission calculated with the NEGF-DFT method for the smaller graphene strips with N = 5 (top), N = 7 (middle) and N = 9 (bottom) in CS (right) and BS (left).

The problem here is that the graphene strips with N = 9 and n ≥ 7 are rather large for being treated at CASSCF level even with a minimal active space. Therefore, we have employed the pseudo-π approach to reduce the full electron system to just the π-electron system.[66] The pseudo-π approach exploits the one-to-one symmetry correspondence between the π orbitals of a sp2-carbon structure and the σ orbitals in an equivalent hydrogen structure. In practice, the carbon atoms in a

geometrically optimized nanographene structure are replaced by hydrogens speeding up considerably the calculations. The approach was successfully employed in the calculation of magnetic and electric response properties.[66-68] On the other hand, in the calculation of the electrical conductance at multideterminant level, the occupied and virtual MOs that built up the EDOs and then the electron transport channels are replaced by natural orbitals (NOs). These NOs are mixed up by the external electric perturbation in the same way as the occupied and virtual orbitals are at single determinant level (see ESI for details).

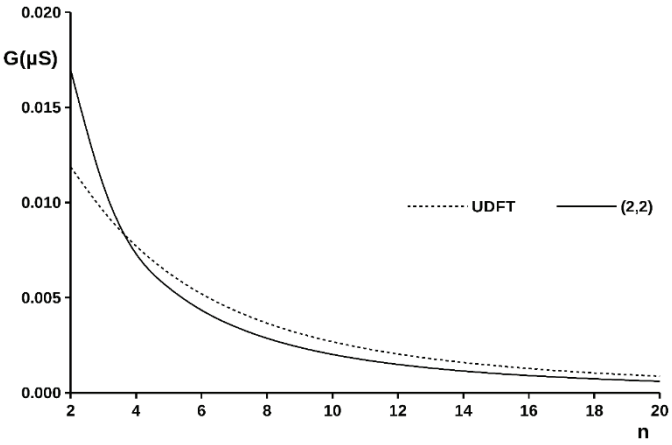

Fig. 6 Electrical conductance vs the number of polyacene units for the ground state of armchair graphene strips with N = 9, calculated with BS-UKS-DFT (dashed lines) and CASSCF(2,2) (solid lines) levels of theory in the frame of the pseudo-π approach.

As mentioned above, the electrical conductance in BS is compared in Fig. 6 with the electrical conductance in the CAS singlet state for the graphene strips with N = 9. Both representations are very similar except for the shortest chains, where some deviations are observed, probably associated with a decrease in the diradical character and then a poor description of the wave function using just two configurations arising from the frontier MOs. In light of this result, we can conclude that multireference and BS calculations give rise to the same picture for the electrical conductance in diradical chains and both predict an exponential decay with the chain length.

4. Conclusions

The results shown in this work confirm the important role played by static correlation in the electron transport properties of molecular chains with diradical character. It points out the previous conclusions obtained from tight-binding models and single-determinant ab initio methods about the relation between diradical character and increasing conductance with length should be revisited using models and methods that properly account for static correlation effects. The alleged exceptional electrical properties of the molecular wires investigated in this work have been predicted with methods that cannot tackle with degeneracies or near degeneracies, such as single determinant RKS-DFT. Herein, we have shown how BS-UKS-DFT properly describes their electronic structure, outcoming the expected conductance-length behavior and other important effects such as the quantum interference associated with aromaticity. Thus, spin symmetry breaking arises as a feasible quantum chemical approach to calculate the electrical conductance in large conducting wires with diradical character given that multireference methods may not be applied here. Among these wires, we can find some of the most promising for the development of molecular electronics, such as organic polymers, graphene strips, non-Kekuléan PAHs or cumulene-like chains. Another question that is still open is the possibility of finding reversed conductance-length behavior in excited states,[49,50] which is a desirable effect for the design of efficient optoelectronic devices.

Conflicts of interest

There are no conflicts to declare.

Acknowledgements

S.G., A.P. and M.M. thanks Xunta de Galicia for financial support through the project GRC2019/24. N.R-B. thanks Xunta de Galicia for a postdoctoral contract.

Notes and references

1 M. Thoss and F. Evers, Perspective: Theory of quantum transport in molecular junctions, *J. Chem. Phys.*, 2018, **148**, 030901.
2 R. A. Rocha, V. M. Garcia Suarez, S. W. Bailey, C. J. Lambert, J. Ferrer and S. Sanvito, Towards molecular spintronics, *Nature Mater.*, 2005, **4**, 335.
3 W. Y. Kim, Y. C. Choi, S. K. Min, Y. Cho and K. S. Kim, Application of quantum chemistry to nanotechnology: electron and spin transport in molecular devices, *Chem. Soc. Rev.*, 2009, **38** 2319.
4 M. L. Perrin, E. Burzuría and H. S. J. van der Zant, Single-molecule transistors, *Chem. Soc. Rev.*, 2015, **44**, 902.
5 C. J. Lambert, Basic concepts of quantum interference and electron transport in single-molecule electronics, *Chem. Soc. Rev.*, 2015, **44**, 875.
6 M. Gilbert and B. Albinsson, Photoinduced charge and energy transfer in molecular wires, *Chem. Soc. Rev.*, 2015, **44**, 845.
7 P. R Bueno and J. J. Davis, Charge transport and energy storage at the molecular scale: from nanoelectronics to electrochemical sensing, *Chem. Soc. Rev.*, 2020, **49**, 7505.
8 V. Popescu, P. Kratzer, P. Entel, C. Heiliger, M. Czerner, K. Tauber, F. Töpler, C. Herschbach, D. V. Fedorov, M. Gradhand, I. Mertig, R. Kováčik, P. Mavropoulos, D. Wortmann, S. Blügel, F. Freimuth, Y. Mokrousov, S. Wimmer, D. Ködderitzsch, M. Seemann, K. Chadova and H. Ebert, Spin caloric transport from density-functional theory, *J. Phys. D: Appl. Phys.*, 2019, **57**, 073001.
9 H. Sadeghi, Theory of electron, phonon and spin transport in nanoscale quantum devices, Nanotech., 2018, **29,** 373001.
10 D. Xiang, X. Wang, C. Jia, T. Lee and X. Guo, Molecular-Scale Electronics: From Concept to Function, *Chem. Rev.*, 2016, **116**, 4318.

11 M. Kiguchi and S. Kaneko, Electron Transport through Single π-Conjugated Molecules Bridging between Metal Electrodes, *ChemPhysChem*, 2012, **13**, 1116.
12 R. J. Nichols and S. J. Higgins, Single-Molecule Electronics: Chemical and Analytical Perspectives. *Ann. Rev Anal. Chem.*, 2015, **8**, 389.
13 K. Manabu, Single-Molecule Electronics: An Introduction to Synthesis, Measurement and Theory, Springer, Singapore, 2016.
14 I. Baldea, Molecular Electronics: An Experimental and Theoretical Approach, Pan Stanford, Singapore, 2015.
15 S. Tajik, H. Beitollahi, F. G. Nejad, I. S. Shoaie, M. A. Khalilzadeh, M. S. Asl, Q. V. Van Le, K. Zhang, H. W. Jang and M. Shokouhimehr, Recent developments in conducting polymers: applications for electrochemistry, *RSC Adv.*, 2020, **10**, 37834.
16 M. Ates, T. Karazehira and A. S. Sarac, Conducting Polymers and their Applications, *Current Phys. Chem.*, 2012, **2**, 224.
17 M. J. González-Tejera, E. Sánchez de la Blanca and I. Carrillo, Polyfuran conducting polymers: Synthesis, properties, and applications, *Synthetic Metals*, 2008, **158**, 165.
18 D. Sheberla, S. Patra, Y. H. Wijsboom, S. Sharma, Y. Sheynin, A.-E. Haj-Yahia, A. H. Barak, O. Gidron, M. Bendikov, Conducting polyfurans by electropolymerization of oligofurans, *Chem. Sci.*, 2015, **6**, 360.
19 D. Thanasamy, D. Jesuraj, S. K. K. Kannan and V. Avadhanam, A novel route to synthesis polythiophene with great yield and high electrical conductivity without post doping process, *Polymer*, 2019, **175**, 32.
20 J. Kerfoot, S. A. Svatek, V. V. Korolkov, T. Taniguchi, K. Watanabe, E. Antolin and P. H. Beton, Fluorescence and Electroluminescence of J-Aggregated Polythiophene Monolayers on Hexagonal Boron Nitride, *ACS Nano*, 2020, **14**, 13886.
21 F. Ghorbani-Zamani, H. Moulahoum, M. Ak, D. Odaci-Demirkol and S. Timur, Current trends in the development of conducting polymers-based biosensors, *TrAC-Trend. Anal. Chem.*, 2019, **118**, 264.
22 R. B. Araujo, A. Banerjee, P. Panigrahi, L. Yang, M. Sjödin, M. Strømme, C. M. Araujo and R. Ahuja, Assessing the electrochemical properties of polypyridine and polythiophene for prospective applications in sustainable organic batteries, *Phys. Chem. Chem. Phys.*, 2017, **19**, 3307.
23 G. Méhes, C. Pan, F. Bencheikh, L. Zhao, K. Sugiyasu, M. Takeuchi, J.-C. Ribierre and C. Adachi, Enhanced Electroluminescence from a Thiophene-Based Insulated Molecular Wire, *ACS Macro Lett.*, 2016, **5**, 781.
24 Y. Li, X. Zhang, D. Wang, F. He, C. Ni, C. and L. Chi, Fabricating sub-100nm conducting polymer nanowires by edge nanoimprint lithography, *J. Colloid Interface Sci.*, 2015, **458**, 300.
25 S. Barman, F. Deng and R. L. McCreery, Conducting polymer memory devices based on dynamic doping, *J. Am. Chem. Soc.*, 2008, **130**, 11073.
26 W. Xu, E. Leary, S. Hou, S. Sangtarash, M. T. Gonzalez, G. Rubio-Bollinger, Q. Wu, H. Sadeghi, L. Tejerina, K. E. Christensen, N. Agrait, S. J. Higgins, C. J. Lambert, R. J. Nichols and H. L. Anderson, Unusual Length Dependence of the Conductance in Cumulene Molecular Wires, *Angew. Chem. Int. Ed.*, 2019, **58**, 8378.
27 Y. Zang, T. Fu, Q. Zou, F. Ng, H. Li, M. L. Steigerwald, C. Colin Nuckolls and L. Venkataraman, Cumulene Wires Display Increasing Conductance with Increasing Length, *Nano Lett.*, 2020, DOI: 10.1021/acs.nanolett.0c03794.
28 M. Koch, F. Ample, C. Joachim and L. Grill, Voltage-dependent conductance of a single graphene nanoribbon, *Nat. Nanotech.*, 2012, **7**, 713.
29 Z. Chen, A. Narita and K. Müllen, Graphene Nanoribbons: On-Surface Synthesis and Integration into Electronic Devices, *Adv. Mater.*, 2020, **32**, 2001893.
30 D. J. Rizzo, M. Wu, H.-Z. Tsai, T. Marangoni, R. A. Durr, A. A. Omrani, F. Liou, C. Bronner, T. Joshi, G. D. Nguyen, G. F. Rodgers, W.-W. Choi, J. H. Jørgensen, F. R. Fischer, S. G. Louieand M. F. Crommie, Length-Dependent Evolution of Type II Heterojunctions in Bottom-Up-Synthesized Graphene Nanoribbons, *Nano Lett.*, 2019, **19**, 3221.
31 Y.-C. Chen, T. Cao, C. Chen, Z. Pedramrazi, D. Haberer, D. G. De Oteyza, F. R. Fischer, S. G. Louie and M. F. Crommie, Molecular bandgap engineering of bottom-up synthesized graphene nanoribbon heterojunctions, *Nat. Nanotech.*, 2015, **10**, 156.
32 K. J. Franke and F. von Oppen, Topological states engineered in narrow strips of graphene, *Nature*, 2018, **560**, 175.
33 N. Richter, Z. Chen, A. Tries, T. Prechtl, A. Narita, K. Müllen, K. Asadi, M. Bonn and M. Kläui, Charge transport mechanism in networks of armchair graphene nanoribbons, *Sci. Rep.*, 2020, **10**, 1988.
34 S. Mishra, D. Beyer, K. Eimre, S. Kezilebieke, R. Berger, O. Gröning, C. A. Pignedoli, K. Müllen, P. Liljeroth, P. Ruffieux, C. Feng and R. Fasel, Topological frustration induces unconventional magnetism in a nanographene, *Nat. Nanotechnol.*, 2020, **15**, 22.
35 J. Li, S. Sanz, J. Castro-Esteban, M. Vilas-Varela, N. Friedrich, T. Frederiksen, D. Peña and J. I. Pascual, Uncovering the triplet ground state of triangular graphene nanoflakes engineered with atomic precision on a metal surface, *Phys. Rev. Lett.*, 2020, **124**, 177201.
36 I. Pozo, Z. Majzik, N. Pavliček, M. Melle-Franco, E. Guitián, D. Peña, L. Gross, and D. Pérez, Revisiting Kekulene: synthesis and single-molecule imaging, *J. Am. Chem. Soc.*, 2019, **141**, 15488.
37 N. Algethami, H. Sadeghi, S. Sangtarash and C. J. Lambert, The Conductance of Porphyrin-Based Molecular Nanowires Increases with Length, *Nano Lett.*, 2018, **18**, 4482.
38 M. H. Garner, W. Bro-Jørgensen, P. D. Pedersen and G. C. Solomon, Reverse Bond-Length Alternation in Cumulenes: Candidates for Increasing Electronic Transmission with Length, *J. Phys. Chem. C*, 2018, **122**, 26777.
39 S. Gil-Guerrero, N. Ramos-Berdullas and M. Mandado, Can aromaticity enhance the electron transport in molecular wires? *Org. Electron.*, 2018, **61**, 177.
40 N. Ramos-Berdullas and M. Mandado, Electronic Properties of p-Xylylene and p -Phenylene Chains Subjected to Finite Bias Voltages: A New Highly Conducting Oligophenyl Structure, *Chem. Eur. J.*, 2013, **19**, 3646.
41 N. Ramos-Berdullas, A. M. Graña, and M. Mandado, Study of electron transport in polybenzenoid chains covalently attached to gold atoms through unsaturated methylene linkers, *Theo. Chem. Acc.*, 2015, **134**, 20.
42 T. Stuyver, S. Fias, F. De Proft, P. Geerlings, Y. Tsuji, and R. Hoffmann, Enhancing the conductivity of molecular electronic devices, *J. Chem. Phys.*, 2017, **146**, 092310.
43 T. Stuyver, T. Zeng, Y. Tsuji, S. Fias, P. Geerlings, and F. De Proft, Captodative Substitution: A Strategy for Enhancing the Conductivity of Molecular Electronic Devices, *J. Phys. Chem. C*, 2018, **122**, 3194.
44 Stuyver, T.; Zeng, T.; Tsuji, Y.; Geerlings, P.; De Proft, F. Diradical Character as a Guiding Principle for the Insightful Design of Molecular Nanowires with an Increasing Conductance with Length, *Nano Lett.*, 2018, **18**, 7298.
45 T. Tada and K. Yoshizawa, Reverse Exponential Decay of Electrical Transmission in Nanosized Graphite Sheets, *J. Phys. Chem. B*, 2004, **108**, 7565.
46 T. Tada and K. Yoshizawa, Molecular design of electron transport with orbital rule: toward conductance-decay free

molecular junctions, *Phys. Chem. Chem. Phys.*, 2015, **17**, 32099.
47 Y. Tsuji, R: Movassagh, S. Datta and R. Hoffmann, Exponential Attenuation of Through-Bond Transmission in a Polyene: Theory and Potential Realizations, ACS Nano **9**, 11109, (2015).
48 Y. Tsuji, K. Okazawa, B. Chen and K. Yoshizawa, Mechanical Control of Molecular Conductance and Diradical Character in Bond Stretching and π-Stack Compression, *J. Phys. Chem. C*, 2020, **124**, 22941.
49 S. Gil-Guerrero, N. Ramos-Berdullas, A. Martín-Pendás, E. Francisco, M. Mandado, Anti-ohmic single molecule electron transport: is it feasible? *Nanoscale Adv.*, 2019, **1**, 1901.
50 S. Gil-Guerrero, A. Peña-Gallego, N. Ramos-Berdullas, A. Martín-Pendás, M. Mandado, Assessing the Reversed Exponential Decay of the Electrical Conductance in Molecular Wires: The Undeniable Effect of Static Electron Correlation, *Nano Lett.*, 2019, **19**, 7394.
51 J. M. Mouesca, Density Functional Theory–Broken Symmetry (DFT–BS) Methodology Applied to Electronic and Magnetic Properties of Bioinorganic Prosthetic Groups. In: Metalloproteins. Methods in Molecular Biology (Methods and Protocols), vol 1122, Fontecilla-Camps J.; Nicolet Y., Humana Press, Totowa, NJ, 2014.
52 L. Noodleman, Valence bond description of antiferromagnetic coupling in transition metal dimers, *J. Chem. Phys.*, 1981, **74**, 5737.
53 L. Noodleman and E. R. Davidson, Ligand Spin Polarization and Antiferromagnetic Coupling in Transition Metal Dimers, *Chem. Phys.*, 1986, **109,** 131.
54 G. Trinquier and J.-P. Malrieu, Kekulé versus Lewis: When Aromaticity Prevents Electron Pairing and Imposes Polyradical Character, *Chem. Eur. J.*, 2015, **21**, 814,.
55 E. Louis, E. San-Fabián, G. Chiappe and J. A. Vergés, Electron enrichment of zigzag edges in armchair–oriented graphene nano–ribbons increases their stability and induces pinning of the Fermi level, *Carbon*, 2019, **154**, 211.
56 J.-P. Malrieu and G. Trinquier, Communication: Proper use of broken-symmetry calculations in antiferromagnetic polyradicals, *J. Chem. Phys.*, 2016, **144**, 211101.
57 S. Gil-Guerrero, M. Melle-Franco, A. Peña-Gallego and M. Mandado, Clar Goblet and Aromaticity Driven Multiradical Nanographenes, *Chem. Eur. J.*, 2020, **26**, 1.
58 M. Kepenekian, J.-M. Gauyacq and N. Lorente, Difficulties in the ab initio description of electron transport through spin filters, *J. Phys.: Condens. Matter*, 2014, **26**, 104203.
59 R. Landauer, Spatial Variation of Currents and Fields Due to Localized Scatterers in Metallic Conduction, *IBM J. Res. Dev.*, 1957, **1**, 223.
60 M. Mandado, and N. Ramos-Berdullas, Analyzing the electric response of molecular conductors using "electron deformation" orbitals and occupied-virtual electron transfer, *J. Comput. Chem.*, 2014, **35**, 1261.
61 N. Ramos-Berdullas, S. Gil-Guerrero and M. Mandado, Transmission channels in the time-energy uncertainty relation approach to molecular conductance: symmetry rules for the electron transport in molecules, *Int. J. Quantum Chem.*, 2018, **118**, e25651.
62 M. J. Frisch, G. W. Trucks, H. B. Schlegel, G. E. Scuseria, M. A. Robb, J. R. Cheeseman, G. Scalmani, V. Barone, G. A. Petersson and H. Nakatsuji, Gaussian 09; Gaussian, Inc.: Wallingford, CT, 2009.
63 R. Dennington, T. Keith and J. Millam, GaussView, version 5, Semichem Inc., Shawnee Mission, KS, 2009.
64 M. Head-Gordon, Characterizing unpaired electrons from the one-particle density matrix, *Chem. Phys. Lett.*, 2003, **372**, 508.
65 M. Deffner, L. Groß, T. Steenbock, B. A. Voigt, G. C. Solomon and C. Herrmann, Artaios - a code for postprocessing quantum chemical electronic structure calculations, available from https://www.chemie.uni-hamburg.de/ac/herrmann/software/index.html, 2008-2017.
66 P. W. Fowler and E. Steiner, Pseudo-π currents: rapid and accurate visualisation of ring currents in conjugated hydrocarbons, *Chem. Phys. Lett.*, 2002, **364**, 259.
67 A. Soncini, R. G. Viglione, R. Zanasi, P. W. Fowler and L. W. Jenneskens, Efficient mapping of ring currents in fullerenes and other curved carbon networks, *C. R. Chim.*, 2006, **9**, 1085.
68 S. Gil-Guerrero, A. Peña-Gallego, and M. Mandado, Detecting Molecular Plasmons by Means of Electron Density Descriptors, *J. Phys. Chem. C*, 2020, **124**, 1585.

The effect of spin polarization on the electron transport of molecular wires with diradical character

Nicolás Ramos-Berdullas, Sara Gil-Guerrero, Ángeles Peña-Gallego and Marcos Mandado*

Department of Physical Chemistry, University of Vigo, Lagoas-Marcosende s/n, 36310, Vigo, Spain

1. Calculation of the electrical conductance from electron deformation orbitals (EDOs)

1.1. Single determinant wave functions

In the Landauer formula[1] the electric conductance, G, is obtained from the product of the quantum conductance, G_0, and the transmission function, T,

$$G = G_0 T \tag{S1}$$

where $G_0 = 2e^2/h$. This equation was originally obtained from scattering theory, but it can be also reached by linear-response theory[2] and the time-energy uncertainty relation approach to the electric conductance.[3] This approach is rooted in the origin of the quantum conductance and its relationship with the time-energy uncertainty principle. Bartra[4,5] derived the expression of G_0 by applying the uncertainty relation to the case of a free electron crossing a monodimensional conductor under the action of a finite bias voltage, ΔV. A generalization to interacting electrons subjected to the external potential created by the nuclei in a molecule gives rise to the following expression,[3]

$$G = \frac{E_{elec}^{(2)} \Delta q_{E-E}}{2h\Delta V} \tag{S2}$$

where, $\Delta q_{E\text{-}E}$ represents the net electronic charge transferred between electrodes upon the action of a bias voltage and $E_{elec}^{(2)}$ is the second order electrostatic energy. To get both

quantities, the difference between the electron density in the electrically perturbed and unperturbed states (ρ^{def}) has to be obtained. Eqns (S3) and (S4) provide expressions of $\Delta q_{E\text{-}E}$ and E_{elec} in terms of ρ^{def}, the latter including also higher order terms which are expected to be unimportant.

$$\Delta q_{E-E} = e\int_{\Omega_E} \rho^{def}(\vec{r})d\vec{r} \tag{S3}$$

$$E_{elec}^{(2)} \approx E_{elec} = e\int \rho^{def}(\vec{r})V(\vec{r})d\vec{r} \tag{S4}$$

It was proven that Eq (S2) can be transformed into Eq (S1) by expressing ρ^{def} with the so-called electron deformation orbitals (EDOs).[6] For a system perturbed by a constant electric field, EDOs can be obtained by diagonalization of the electron deformation density matrix. The electron deformation density matrix is defined as,

$$\mathbf{D}^{def} = \mathbf{D}^{l} - \mathbf{D}^{0} \tag{S5}$$

where, $\mathbf{D}^{l}$ and $\mathbf{D}^{0}$ are, respectively, density matrices for the perturbed and unperturbed systems on the basis of the unperturbed molecular orbitals. Then, the EDOs represent the eigenfunctions of $\mathbf{D}^{def}$, each with its corresponding eigenvalue. Denoting the eigenvector matrix by $\mathbf{U}$ and the set of unperturbed molecular orbitals by $\{\chi_i\}$, each EDO is given by,

$$\xi_i = \sum_j u_{ij}\chi_j \tag{S6}$$

They represent the eigenchannels for the electrically induced electron transport in molecules and are grouped in pairs of eigenfunctions with the same absolute eigenvalue but opposite sign. Positive and negative EDOs of a given pair, ξ_k^+ and ξ_k^-, are, respectively, electron and hole functions within the same electron transport channel, which is mathematically represented by the 2x2 matrix $\mathbf{\Theta}_k$,

$$\mathbf{\Theta}_k = n_k^{1/2}\begin{pmatrix} \xi_k^+ & 0 \\ 0 & i\xi_k^- \end{pmatrix} \tag{S7}$$

Thus, the total electron deformation density can be obtained from the traces of the $\mathbf{\Theta}_k$ matrix products,

$$\Delta\rho = 2\sum_{k=1}^{N_{CH}} \mathrm{Tr}\left(\mathbf{\Theta}_k^t \mathbf{\Theta}_k\right) \tag{S8}$$

Combining Eqs (S2), (S3), (S4) and (S6) leads, after some algebraic manipulations,[3] to the following expression for the electric conductance,

$$G = \frac{2e^2}{h} \mathrm{Tr}\left(\mathbf{t}^t \mathbf{t}\right) \tag{S9}$$

with the elements of the matrix $\mathbf{t}$ given by,

$$\mathbf{t}_{ij} = \left(\int \mathrm{Tr}\left(\mathbf{\Theta}_i^t \hat{\mathbf{r}}^{\mathrm{d}} \mathbf{\Theta}_i\right) d\tau \int_{\Omega_E} \mathrm{Tr}\left(\mathbf{\Theta}_j^t \mathbf{\Theta}_j\right) d\tau \right)^{1/2} \tag{S10}$$

In Eq (S8), $\hat{\mathbf{r}}^{\mathrm{d}}$ represents the position operator scaled to the distance, d, between the two points where the bias voltage is applied and the second integral on the rhs is restricted to the electrode region.

Since the EDOs are constructed as linear combinations of MOs, the role played by occupied and virtual orbitals on the electron transport can be analyzed. Moreover, the electron and hole densities associated with a given transmission channel can be represented in real space.

1.2 Multideterminant wave functions

For multideterminant wave functions, like the wave function obtained from the configuration interaction (CI) method,

$$\Psi_{CI} = \sum_{I=1}^{ND} c_I \Psi_I \tag{S11}$$

where Ψ_I represents one of *ND* possible determinants constructed from the combination of *N* electrons in *n* occupied and virtual Hartree-Fock spin orbitals, the electron density, ρ, may be expressed with the natural orbitals, ψ_i, and the corresponding occupation numbers, n_i.

$$\rho = \left\langle \Psi_{CI}^{\ *} \left| \hat{\rho} \right| \Psi_{CI} \right\rangle = \sum_{i=1}^{NNO} n_i \psi_i \qquad \text{(S12)}$$

These natural orbitals are the eigenvectors and eigenvalues of the electron density matrix. EDOs and electron transport channels given in Eqs (S6) and (S7) can then be constructed with these natural orbitals in the same way as in the single determinant case with occupied and virtual MOs. This does not imply any extra computational cost in the subsequent calculation of the electrical conductance.

2. Electrical conductance in open-shell singlet, triplet and broken-symmetry states

First, we show here how the electric conductance for open-shell singlet (OS), triplet (T) and broken symmetry (BS) states converge to the same value for perfect diradical chains.

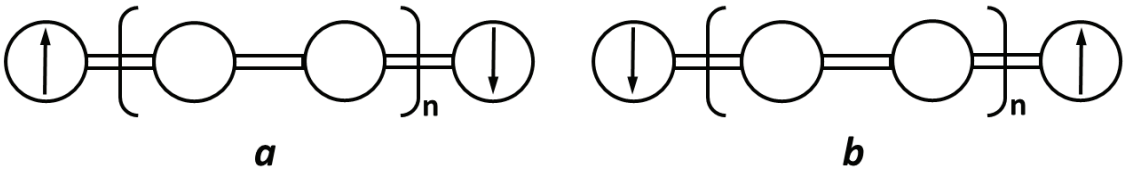

Fig. S1 Pictorial representation of the two BS states in a diradical chain with n+2 repeating units.

In Fig. S1, we can see a pictorial representation of the two possible BS states in a given diradical chain. To form these two BS states, the unpaired spin up and spin down electrons, localized at the chain ends, are exchanged, so that forming two degenerate states. Let's label these degenerate BS states as $\Psi_{BS}^{\uparrow\downarrow}$ (***a*** in Fig. S1) and $\Psi_{BS}^{\downarrow\uparrow}$ (***b*** in Figure

S1). They are not eigenstates of the spin operator squared, $\mathbf{S^2}$. Spin adapted configurations for the OS and one of the T states may be built from linear combinations of them.[7]

$$\Psi_S = 2^{-1/2}\left[\Psi_{BS}^{\uparrow\downarrow} - \Psi_{BS}^{\downarrow\uparrow}\right] \qquad \Psi_T = 2^{-1/2}\left[\Psi_{BS}^{\uparrow\downarrow} + \Psi_{BS}^{\downarrow\uparrow}\right] \tag{S13}$$

These states are then eigenstates of $\mathbf{S^2}$ and cannot be represented by just one single Slater determinant but the two determinants of the BS states. Alternatively, we can also represent the BS states as linear combinations of Ψ_S and Ψ_T

$$\Psi_{BS}^{\uparrow\downarrow} = 2^{-1/2}\left[\Psi_S + \Psi_T\right] \qquad \Psi_{BS}^{\downarrow\uparrow} = 2^{-1/2}\left[\Psi_T - \Psi_S\right] \tag{S14}$$

We can go on with any of the two BS states represented above, both will lead us to the same result. Applying the density operator on state $\Psi_{BS}^{\uparrow\downarrow}$ and considering the orthogonality of OS and T states, we have,

$$\left\langle \Psi_{BS}^{\uparrow\downarrow *} \left| \hat{\rho} \right| \Psi_{BS}^{\uparrow\downarrow} \right\rangle = 2^{-1}\left[\left\langle \Psi_S{}^* \left| \hat{\rho} \right| \Psi_S \right\rangle + \left\langle \Psi_T{}^* \left| \hat{\rho} \right| \Psi_T \right\rangle\right] \tag{S15}$$

which tell us the electron density of the BS states is the average of the OS and T electron densities. We can then obtain the electron density of the OS state, which is not accessible from a single determinant DFT calculation, indirectly from the T and BS states.

$$\left\langle \Psi_S{}^* \left| \hat{\rho} \right| \Psi_S \right\rangle = 2\left\langle \Psi_{BS}^{\uparrow\downarrow *} \left| \hat{\rho} \right| \Psi_{BS}^{\uparrow\downarrow} \right\rangle - \left\langle \Psi_T{}^* \left| \hat{\rho} \right| \Psi_T \right\rangle \tag{S16}$$

In the case of the T, we cannot obtain the state given in Eq (S13) but any of the other two degenerate states with two spin up or spin down electrons, respectively, from a single determinant unrestricted DFT calculation.

The one-electron density matrix for the OS can be represented on the basis of the so-called magnetic orbitals from the BS state or the spin-orbitals from the T. Using the former, the one-electron density matrix for the OS is given by,

$$\mathbf{D_S} = 2\mathbf{D_{BS}} - \mathbf{O}^{\mathbf{t}}_{\mathbf{T}\rightarrow\mathbf{BS}}\mathbf{D_T}\mathbf{O}_{\mathbf{T}\rightarrow\mathbf{BS}} \tag{S17}$$

where $\mathbf{O}_{T\rightarrow BS}$ is the orbital transformation matrix from the T spin orbitals to the BS magnetic orbitals. With the density matrix before and after the application of the perturbation, we can proceed with the calculation of the electrical conductance following the method explained in section 1.1. However, in strongly diradical chains, where the overlap between the spin up and spin down magnetic orbitals is negligible,[8] the differences in the electron density and the energy of the OS, T and BS states are also negligible. As proof, we have represented in Fig. S2 the electrical conductance for the BS and T states in the series of dimethylene polyphenylene, dimethylene polyfuran and dimethylene polythiophene.

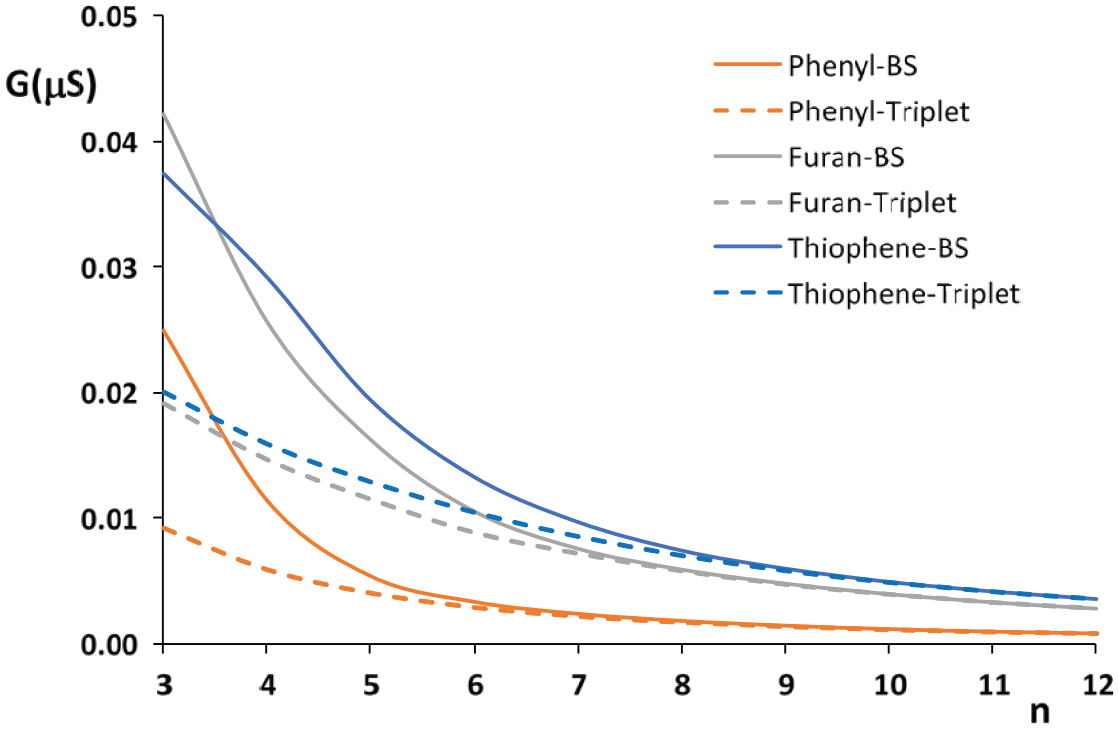

Fig. S2 Electrical conductance vs the number of aromatic units for the BS (solid lines) and T (dashed lines) states of dimethylene polyphenylene (orange), dimethylene polyfurane (grey) and dimethylene polythiophene (blue) chains.

As can be observed, the conductance profiles are identical for long chains with strong diradical character. Taking into account that BS-UKS-DFT performs well in these cases,

we have analyzed in the body of the letter directly the electrical conductance in the BS state instead of the OS.

3. Energy gaps between different spin states

In this section, the energies of the closed-shell singlet (CS), BS and T states are compared in three different tables for the organic polymeric (Table S1), quinoid-cumulenes (Table S2), and graphene strips (Table S3). For perfect diradical chains the BS-T energy gap is negligible. This happens in dimethylene polyphenylene with n > 4, dimethylene polyfurane with n > 7 and dimethylene polythiophene with n > 8, in agreement with the conductance curves represented in Fig. S2. In quinoid-cumulenes, the diradical character is significantly lower but the BS is the lowest energy state for all the chains. In graphene strips with N = 5, no BS state was found and the T state is significantly less stable than the CS. In strips with N = 7 and N = 9, the BS state is always more stable than the CS, and an almost perfect diradical character is reached for chains with n > 10 and n > 5, respectively.

Table S1. Energies for the closed-shell (**CS**), broken-symmetry (**BS**) and triplet (**T**) lower energy states in dimethylene polyphenylene (**Phenyl**), dimethylene polyfurane (**Furan**) and dimethylene polythiophene (**Thiophene**) chains. Absolute energies in Hartrees are given for **CS**, whereas those of **BS** and **T** are relative to **CS** and given in eV.

Phenyl	CS	BS	T
3	-1311.04796	-0.390	-0.351
4	-1542.01020	-0.728	-0.722
5	-1772.97874	-0.910	-0.909
6	-2003.95141	-0.986	-0.986
7	-2234.92569	-1.014	-1.017
8	-2465.90061	-1.030	-1.030
9	-2696.87559	-1.038	-1.038
10	-2927.85094	-1.044	-1.044
11	-3158.82605	-1.047	-1.047

12	-3389.80151	-1.051	-1.051
Furan			
3	-1304.58508	-0.004	0.301
4	-1533.43531	-0.125	-0.015
5	-1762.28692	-0.301	-0.260
6	-1991.13987	-0.461	-0.445
7	-2219.99457	-0.589	-0.583
8	-2448.85093	-0.669	-0.666
9	-2677.70845	-0.725	-0.724
10	-2906.56670	-0.759	-0.759
11	-3135.42553	-0.776	-0.776
12	-3364.28440	-0.795	-0.795
Thiophene			
3	-2273.55860	-0.001	0.390
4	-2825.39958	-0.051	0.106
5	-3377.24151	-0.179	-0.115
6	-3929.08406	-0.324	-0.297
7	-4480.92749	-0.457	-0.446
8	-5032.77213	-0.563	-0.558
9	-5584.61809	-0.635	-0.633
10	-6136.46511	-0.679	-0.678
11	-6688.31276	-0.706	-0.705
12	-7240.16078	-0.719	-0.719

Table S2. Energies for the closed-shell (**CS**), broken-symmetry (**BS**) and triplet (**T**) lower energy states in quinoid-cumulenes with phenyl (**QDC**) and anthracene (**AC**) as central aromatic units. Absolute energies in Hartrees are given for **CS**, whereas those of **BS** and **T** are relative to **CS** and given in eV.

QDC	CS	BS	T
1	-841.68742	-0.060	-0.004
2	-993.83739	-0.074	-0.031
3	-1145.99180	-0.084	-0.051
4	-1298.14791	-0.092	-0.067
5	-1450.30477	-0.095	-0.079
AC			

1	-1148.62190	-0.008	0.113
2	-1300.77173	-0.018	0.069
3	-1452.92592	-0.028	0.041
4	-1605.08179	-0.037	0.018
5	-1757.23845	-0.045	0.000

Table S3. Energies for the closed-shell (**CS**), broken-symmetry (**BS**) and triplet (**T**) lower energy states in armchair graphene strips with N = 5 (**Naphthalene**), N = 7 (**Anthracene**) and N = 9 (**Tetracene**). For N = 9 and n ≤ 8, absolute energies in Hartrees are given for **CS**, whereas those of **BS** and **T** are relative to **CS** and given in eV. For N = 9 and n > 8, calculations of **CS** did not converge and the data for **BS** correspond to absolute energies given in Hartrees, whereas those of **T** are relative to **BS** and given in eV.

Naphtalene	**CS**	**BS**	**T**
2	-769.4602	0.000	1.877
3	-1152.9990	0.000	1.401
4	-1536.5381	0.000	1.162
5	-1920.0774	0.000	1.023
6	-2303.6166	0.000	0.934
7	-2687.1559	0.000	0.873
8	-3070.6952	0.000	0.831
9	-3454.2346	0.000	0.801
10	-3837.7739	0.000	0.778
11	-4221.3132	0.000	0.762
12	-4604.8525	0.000	0.749
13	-4988.3918	0.000	0.739
14	-5371.9311	0.000	0.732
15	-5755.4705	0.000	0.726
16	-6139.0098	0.000	0.722
17	-6522.5491	0.000	0.718
18	-6906.0884	0.000	0.715
19	-7289.6277	0.000	0.713
20	-7673.1671	0.000	0.712
Anthracene			
2	-1075.5767	0.000	0.829
3	-1611.5864	-0.021	0.330
4	-2147.5985	-0.106	0.055

5	-2683.6120	-0.201	-0.123
6	-3219.6265	-0.287	-0.249
7	-3755.6420	-0.358	-0.340
8	-4291.6581	-0.415	-0.405
9	-4827.6749	-0.457	-0.452
10	-5363.6921	-0.488	-0.485
11	-5899.7097	-0.510	-0.508
12	-6435.7275	-0.525	-0.524
13	-6971.7455	-0.536	-0.535
14	-7507.7636	-0.543	-0.543
15	-8043.7818	-0.549	-0.549
16	-8579.8000	-0.553	-0.553
17	-9115.8183	-0.556	-0.556
18	-9651.8366	-0.559	-0.559
19	-10187.8550	-0.561	-0.561
20	-	-	-
Tetracene			
2	-1381.6923	-0.063	0.233
3	-2070.1767	-0.293	-0.221
4	-2758.6668	-0.464	-0.443
5	-3447.1602	-0.562	-0.555
6	-4135.6555	-0.613	-0.611
7	-4824.1518	-0.640	-0.639
8	-5512.6486	-0.655	-0.655
9		-6201.1700	0.000
10		-6889.6673	0.000
11		-7578.1646	0.000
12		-8266.6619	0.000
13		-8955.1593	0.000
14		-9643.6566	0.000
15		-10332.1539	0.000
16		-11020.6512	0.000
17		-11709.1485	0.000
18		-12397.6458	0.000
19		-13086.1432	0.000

20	-13774.6402	-0.008

4. Diradical character in graphene strips from CASSCF(2,2) calculations

In this section, the diradical character in the different graphene strips is compared using minimal active space CASSCF calculations with the help of the pseudo-π approach.[9] The pseudo-π approach exploits the one-to-one symmetry correspondence between the π orbitals of an sp2-carbon structure and the σ orbitals in an equivalent hydrogen structure. In practice, the carbon atoms in a geometrically optimized sp2-carbon structure are replaced by hydrogens speeding up considerably the calculations. The resulting pseudo-π structure has MOs with the same symmetry properties as the π MOs of the real carbon structure.

The number of effectively unpaired electrons (N_U)[10] measures the radical character, being comprised between 0 and 2 in the case of partially diradical structures. This index is obtained from the occupation numbers, n_i, of the natural orbitals within the active space, AS, in a CASSCF calculation.

$$N_U = \sum_{i \in AS} n_i^2 \left(2 - n_i\right)^2 \qquad \text{(S17)}$$

In Table S4, the N_U values for the pseudo-π structures of the graphene strips are collected. They clearly reflect there is no diradical character in the strips with N = 5, whereas strips with N = 9 are strongly diradical even in relatively short chains. Strips with N = 7 represent an intermediate situation. All of this is in agreement with the BS-UKS-DFT energy gaps shown in the previous section.

Table S4. N_U values obtained at the CASSCF(2,2) level using the pseudo-π approach for the armchair graphene strips with N = 5 (**Naphthalene**), N = 7 (**Anthracene**) and N = 9 (**Tetracene**).

	Naphthalene	**Anthracene**	**Tetracene**
2	0.06	0.06	0.32
3	0.06	0.05	1.52
4	0.06	0.03	1.89
5	0.06	1.05	1.97
6	0.06	1.86	1.99
7	0.01	1.94	2.00
8	0.06	1.97	2.00
9	0.06	1.99	2.00
10	0.06	1.99	2.00
11	0.06	2.00	2.00
12	0.06	2.00	2.00
13	0.06	2.00	2.00
14	0.00	2.00	2.00
15	0.00	2.00	2.00
16	0.00	2.00	2.00
17	0.00	2.00	2.00
18	0.00	2.00	2.00
19	0.00	2.00	2.00
20	0.00	2.00	2.00

5. Tetraphenyl cumulenes

In this section, we present calculations carried out for the tetraphenyl cumulenes depicted in Fig. S3.

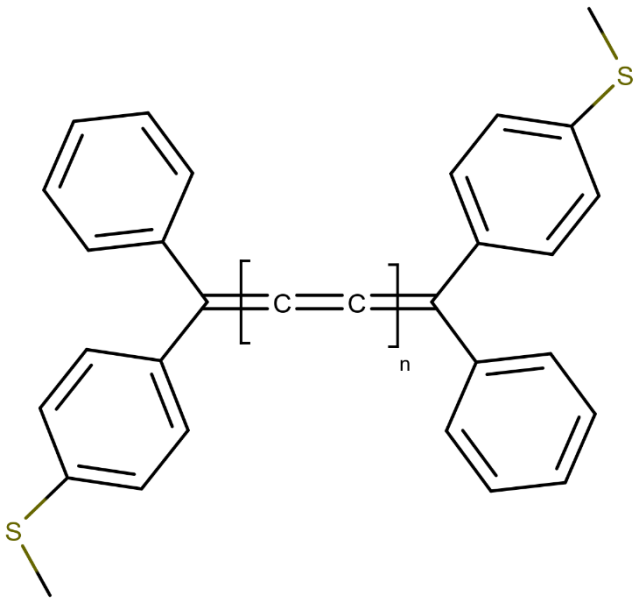

Fig. S3 Tetraphenyl cumulene chains studied in references 11 and 12 **C4** (n=1), **C6** (n=2) and **C8** (n=3).

The electron transport in these systems has been studied experimentally using STM, obtaining an unexpected increase of the electrical conductance with the length of the cumulene chain.[11,12] Transmission calculations using NEGF-DFT reproduce the experimental behavior.[11,12] Herein, we have first investigated if this behavior is connected to diradical character. In Table S5, the energies of the CS, BS and T states are collected. CS state is significantly more stable than T state in all cases, so that the calculations for the BS state converge to the CS. Therefore, these systems do not seem to display a perceptible diradical character and the increase of the electrical conductance with the length may be associated with other electronic or geometrical features.

Table S5. Energies for the closed-shell (**CS**), broken-symmetry (**BS**) and triplet (**T**) lower energy states in the tetraphenyl cumulenes depicted in Figure S4. Absolute energies in Hartrees are given for **CS**, whereas those of **BS** and **T** are relative to **CS** and given in eV.

	CS	**BS**	**T**
C4	-1953.4640	0.000	1.019
C6	-2029.5845	0.000	0.656

C8	-2105.7080	0.000	0.464

Herein, the electrical conductance obtained for the same chains using EDOs is depicted in Fig. S4. The calculations were performed on geometrically optimized chains attached by the sulphur atoms to clusters containing twenty gold atoms. The bond distances between sulphurs and the apical centers of the clusters were also optimized as well as the S-Au-C bond angles. As can be observed, a small increase of the conductance with the length of the central cumulene chain is also predicted using EDOs.

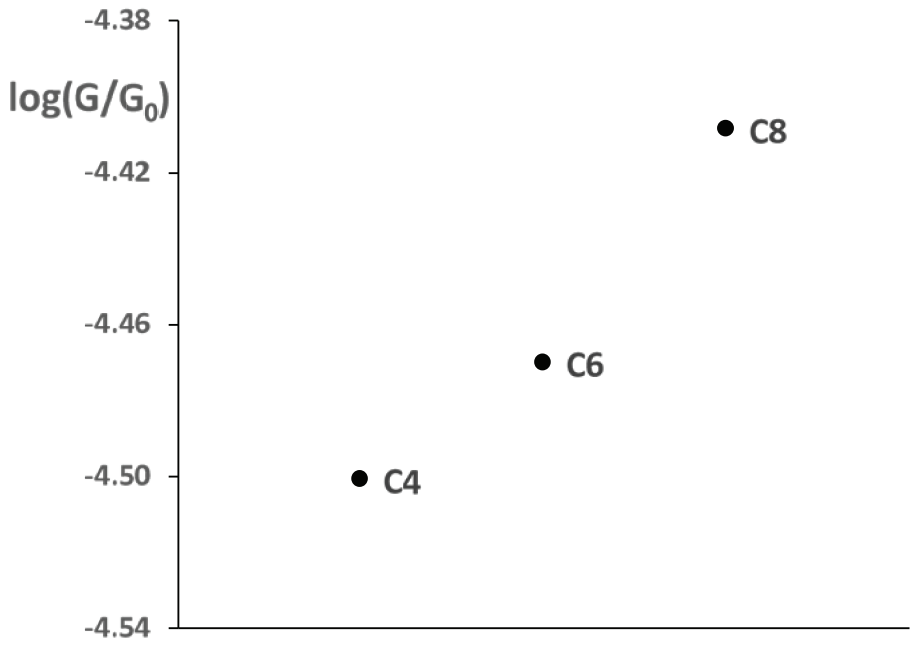

Fig. S4 Electrical conductance calculated at a voltage of 100 mV for the tetraphenyl cumulene chains depicted in Fig. S3 attached to clusters of 20 gold atoms. The conductance is given relative to the quantum conductance G_0 using a logarithmic scale.

References

1 R. Landauer, Spatial Variation of Currents and Fields Due to Localized Scatterers in Metallic Conduction, *IBM J. Res. Dev.*, 1957, **1**, 223.

2 H. D. Cornean, A. Jensen and V. J. Moldoveanu, *Math. Phys.*, 2005, **46**, 042106.

3 N. Ramos-Berdullas, S. Gil-Guerrero and M. Mandado, Transmission channels in the time-energy uncertainty relation approach to molecular conductance: symmetry rules for the electron transport in molecules, *Int. J. Quantum Chem.*, 2018, **118**, e25651.

4 I. P. Batra, Origin of conductance quantization, *Surf. Sci.*, 1998, **395**, 43.

5 I. P. Batra, From uncertainty to certainty in quantum conductance of nanowires, *Solid State Commun.*, 2002, **124**, 463.

6 M. Mandado, and N. Ramos-Berdullas, Analyzing the electric response of molecular conductors using "electron deformation" orbitals and occupied-virtual electron transfer, *J. Comput. Chem.*, 2014, **35**, 1261.

7 J. M. Mouesca Density Functional Theory–Broken Symmetry (DFT–BS) Methodology Applied to Electronic and Magnetic Properties of Bioinorganic Prosthetic Groups. In: Metalloproteins. Methods in Molecular Biology (Methods and Protocols), vol 1122, Fontecilla-Camps J.; Nicolet Y., Humana Press, Totowa, NJ, 2014.

8 F. Neese, Definition of corresponding orbitals and the diradical character in broken symmetry DFT calculations on spin coupled systems, *J. Phys. Chem. Sol.*, 2004, **65** 781.

9 P. W. Fowler and E. Steiner, E. Pseudo-π currents: rapid and accurate visualisation of ring currents in conjugated hydrocarbons, *Chem. Phys. Lett.*, 2002, **364**, 259.

10 M. Head-Gordon, Characterizing unpaired electrons from the one-particle density matrix, *Chem. Phys. Lett.*, 2003, **372**, 508.

11 W. Xu, E. Leary, S. Hou, S. Sangtarash, M. T. Gonzalez, G. Rubio-Bollinger, Q. Wu, H. Sadeghi, L. Tejerina, K. E. Christensen, N. Agrait, S. J. Higgins, C. J. Lambert, R. J. Nichols and H. L. Anderson, Unusual Length Dependence of the Conductance in Cumulene Molecular Wires. *Angew. Chem. Int. Ed.*, 2019, **58**, 8378.

12 Y. Zang, T. Fu, Q. Zou, F: Ng, H. Li, M. L. Steigerwald, C. Colin Nuckolls, L. Venkataraman, Cumulene Wires Display Increasing Conductance with Increasing Length, *Nano Lett.*, 2020, DOI: 10.1021/acs.nanolett.0c03794.